Jurnal Teknologi

Full Paper

STUDY THE INFLUENCE OF WELDING PARAMETERS BY TAGUCHI'S DESIGN ON THE MECHANICAL PROPERTIES OF WELDED MILD STEEL (S235JR)

Saleh Suliman Saleh Elfallah*

Engineering Faculty, Libyan International Medical University, Benghazi, Libya

*Corresponding author
saleh.elfallah@limu.edu.ly

Article history
Received
17 December 2022
Received in revised form
6 April 2023
Accepted
11 April 2023
Published Online
25 June 2023

Graphical abstract

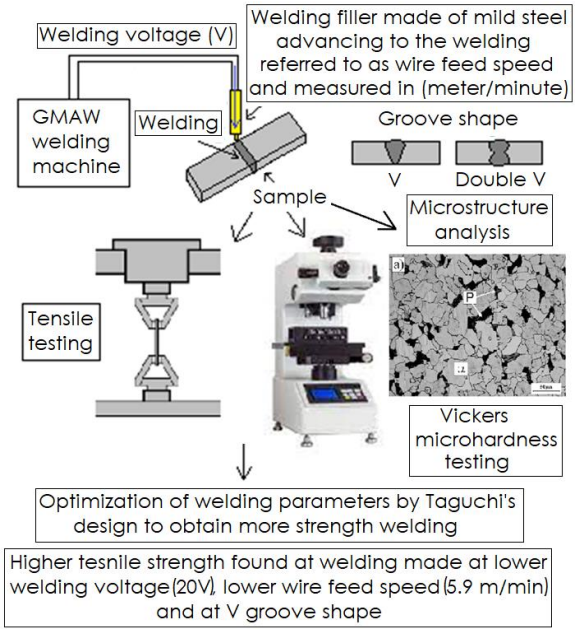

Abstract

Gas metal arc welding is a leading process in fusion welding with increased productivity and good quality. The welding parameters are crucial in determining welding quality, cost, and productivity. In this study, mild steel with a 10-mm-thick sheet was welded by gas metal arc welding under predetermined parameters of welding voltage, wire feed speed, and groove shape. The analysis made by Taguchi's design to investigate the effect of these parameters on tensile strength and Vickers micro-hardness of welding. The microstructure of the fusion zone and heat-affected zone is analyzed to monitor their change concerning the mechanical properties. The results showed that tensile strength decreased with decreased hardness. Also, the tensile strength and hardness were higher (a maximum of 305 MPa and 2170 HVN) at welding made at a lower voltage (20 volts), lower wire feed speed (5.9 m/min), and V-shaped base metal groove. The increased precipitation of perlite structure was shown during welding, which has lower tensile strength and hardness. Widmanstatten ferrite and coarser a-ferrite were presented for welding with a lower cooling time. Taguchi's design showed that voltage at 20 volts has the highest effect on tensile strength, followed by wire feed speed at 5.9 m/min and V-shaped welding.

Keywords: Mild steel, Gas metal arc welding, Taguchi's design, mechanical properties, microstructure

1.0 INTRODUCTION

Gas metal arc welding (GMAW) is a versatile welding technique that is favored in fabrication because of its high productivity and mechanization [1, 2]. It is highly recommended for joining steel base metals due to its low operating cost, ease of use, and good adaptability [3, 4]. GMAW is increasingly utilized in industry due to its application to all positions. Which make it easily automated and integrated into robotic system production and produce good quality welds [1, 5, 6]. These advantages of GMAW have motivated researchers to study the process in detail [5, 6]. It has a variety of uses for steel structures, hydraulic electro-generating, and food mechanisms [4]. It is famous for the welding of plate sheets with a variety of thicknesses, especially thin sheets, due to the ease of start-up and stoppage and its capability of achieving higher productivity [6].

GMAW uses a consumable electrode or welding filler shielded by externally supplied gas. The common shielding gases used in GMAW are argon

(Ar), carbon dioxide (CO_2), and a mixture of both. The shielding gas protects the molten welding from air contamination and influences the welding arc and its stability and metal transfer [5].

In order to reach optimum welding quality, the welding parameters had to be set correctly [6]. Parameters such as welding voltage, welding current, wire feed speed (WFS), welding speed, electrode extension or stick-out, electrode diameter, and other parameters are studied by researchers and manufacturers to optimize the welding process [7, 8].

Welding is an expensive process due to the high cost of materials, operation, and other ancillary costs. For that, the welding has to be well prepared and count. In order to lower the expenses, there are numerous techniques for optimizing the process, such as the Design of Experiments (DoE), Taguchi's design, and ANOVA analysis. Taguchi's design was proposed by several researchers for welding process optimization due to the fact that it uses an orthogonal array experimentation design with a minimum number of runs or experiments [9]. It is widely used to optimize engineering and manufacturing processes. It Taguchi design utilizes performance measurement statistics called signal-to-noise (S/N). It compares the mean of the response or the results (signal) to the standard deviation, which is the noise. The ratio depends on the characteristics and quality of the product and the desired output, whether to maximize (higher is better), minimize (lower is better), or nominally target the target (nominal is better) [10, 11, 12].

Mild steel is wiedly is in industry and in some industrial sectors is considered the main material for construction. However, to achieve the optimal welding parameters for more effective welds has been manufacturers endeavor always. The mechanical properties of welding is an important aspect for the consistenly of such welding products [9, 13].

Researchers have studied the effect of welding parameters according to Taguchi's design on the mild steel welding tensile strength and hardness [14, 15, 16, 17, 18, 19, 20, 21]. For instance, in the study on welding penetration depth, Ogbonna *et al*. (2023) found that welding voltage has the highest influence on the tensile strength of AISI 1008 mild steel heterogeneous welding over welding current and gas flow rate [14]; Om Prakash *et al*. (2019) found that welding WFS had a higher effect on the tensile strength of AISI 11040 steel welding over the welding voltage and welding speed [15]; and Assefa *et al*. (2022) concluded that welding current has a higher effect on the tensile strength and hardness of dissimilar mild steels [16]. Another study by Khan *et al*. (2020) found that welding current has a higher influence on EN8 mild steel with dissimilar welding hardness [17]; Khamari *et al*. (2019) stated that a higher current contributed to a higher welding tensile strength [18]. Previous similar studies concluded that tensile strength increased with decreasing welding voltage, welding current, and WFS [19, 20, 21]. The groove shape was also reported to affect the mechanical properties of welding, where V-shaped welding obtained higher tensile strength and hardness than double V-shaped welding [20].

The relationship between tensile strength and hardness was reported before [19, 20, 21]. Calderón *et al*. (2021) concluded that the tensile strength and hardness of FZ and HAZ were also studied because they affect the mechanical properties of welding due to the different properties of the welding and adjacent regions [22]. Other studies reported the hardness and microstructure of the welding regions-the fusion zone (FZ) and the heat affected zone (HAZ)—and related their effect on the tensile strength of welding. Luo *et al*. (2020) stated in a study on 304 stainless steel welding that HAZ has a higher hardness than FZ. It is because the first has a smaller δ-ferrite grain structure due to having been exposed to a higher heat input than austenitic grains at HAZ. The study also concluded that higher welding heat input increased the tensile strength of welding [23]. Sabri (2021) study on 6061 aluminum alloy welding found that FZ has lower hardness than HAZ [24]. On the contrary, Khamari *et al*. (2019) in a study on mild steel welding reported that FZ, because of the faster solidification due to lower heat input, has higher hardness due to the formation of fine grains of martensitic and bainitic, while the hardness decreased at the coarsening regions (HAZ and base metal), which form ferritic and perlitic structures [18]. These studies stated the effect of welding heat input on the microstructure, which affects hardness and consequently the tensile strength of welding. However, it is not clear how the changes in microstructure and hardness affect the final transverse tensile strength of welding as reported in these studies. In comparison on the transverse tensile strength between the mild steel welding and the base metal. The welding was found to have lower tensile strength, although it has higher hardness [19, 20, 21]. Other studies reported that the welded joint has higher tensile strength than base metal but lower toughness [18, 25]. Sankar *et al*. (2021) have elucidated that this is due to the formation of fine lamellar pearlite with acicular ferrite and Widmanstatten ferrite structure in the welding region [25].

In this paper, a study on the effect of the microstructure on the hardness and transverse tensile strength of mild steel welded at variations of welding parameters will be demonstrated. Mild steel is the main steel utilized in industry in Benghazi, Libya. The optimization and influence of welding parameters (welding voltage, WFS, and groove shape) on the results will be analyzed. The effect of the groove shape parameter was included due to its significant influence on the welding in a previous study [19]. The objective is to obtain the best practical conditions for stronger, more effective, and more consistent welding.

2.0 METHODOLOGY

Mild steel is the material utilized for welding. It follows the European standard EN 10025-2, grade S235JR (1.0038). The welding filler used for welding is Nexus copper-coated mild steel welding wire grade AWS ER70 S-6, according to the American Welding Society, with a thickness of 0.045 in (1.143 mm). The material composition is shown in Table 1, and Table 2 shows their mechanical properties. The Vickers microhardness was measured for the base metal, and an average was taken. The mild steel composition and properties were taken from theworldmaterial.com, while the welding filler data was taken from weldwire.net. It is brought from the local market in sheets measuring 1000 mm by 800 mm and 10 mm in thickness. It is prepared by a CNC laser cutter router in the Tasamim Workshop in Benghazi. The sample preparation follows ASTM E8/E8M-22 [26] for the tensile testing with a base metal thickness of 10 mm, as seen in Figure 1. The preparation of base metal groove shaping is done by a JMTC electric bench grinder with water as a coolant at the College of Mechanical Engineering Technology. Also, other samples were prepared for hardness and microstructure testing using a similar technique. The welding was conducted in the welding lab at ambient temperature at the Saad Elkarimi Institute of Technology in Benghazi. The welding sample fixation for V-shaped base metal groove prior to welding process in Figure 2. A mixture of 82% argon and 18% carbon dioxide is the shielding gas utilized, with a gas flow rate of 18 ml/min. The current is estimated to be 120 amperes at 20 volts and 270 amperes at 27.5 volts. The welding is done manually with both hands at an approximate speed of 150 mm per minute. The samples are fixed to a workbench with clamps. The number of passes made for each groove-shaped base metal is shown in Figure 3 at higher WFS. Knowing that at lower WFS more passes were applied. The experiment setup as seen in Table 3 follows the Taguchi design's orthogonal array of three parameters (2^3) with two levels at each, resulting in a total of four experiments (L4). However, Minitab 18® couldn't estimate the experiment's coefficient with such a design. Therefore, Taguchi's design allows for experiments to be extended to 8 since L4 was not sufficient to generate an ANOVA analysis. This method is known as Taguchi's L8 array, as seen in Table 4.

Table 1 The chemical compositions of the metal joint and welding wire used in the experiment [27, 28]

Component	Composition (%)								
	C	Mn	S	Ni	Cr	P	Si	Cu	Fe
Base metal	0.17	1.4	0.025	0.012	-	0.025	-	0.55	Balanced
Welding filler	0.09	1.65	0.018	0.15	0.15	0.012	0.95	0.35	Balanced

Table 2 The tensile properties and hardness of base metal and welding filler [27, 28]

Component	Tensile properties			Hardness properties	
	Yield strength	Tensile strength	Elongation (%)	Brinell hardness	Vickers micro-hardness
Base metal	235	360-510	26	≤120 HBW	≈2025 HV
Welding filler	452 MPa (65.5 ksi)	538 MPa (78 ksi)	24	-	-

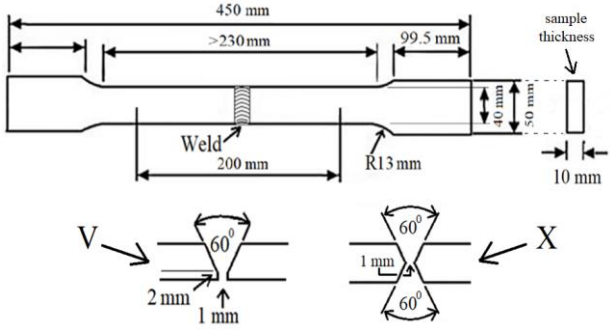

Figure 1 Tensile test dimensions according to ASTM E8/E8M-22 [26]

Figure 2 V-shaped base metal groove sample fixing prior to welding

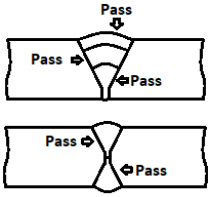

Figure 3 Welding passes

Table 3 Experiment setup for the welding process

Code	Parameters	Unit	Level 1	Level 2
A	Voltage	Volts	20	30
B	Wire feed speed (WFS)	m/min	5.9	10.6
C	Base metal Groove shape	-	V	Double V

Table 4 Orthogonal array parameters assignments to experimental array columns

A	B	C
1	1	1
1	1	2
1	2	1
1	2	2
2	1	1
2	1	2
2	2	1
2	2	2

The tensile test was carried out on a Shimadzu UEH-20 universal testing machine at the Libyan Iron and Steel Company in Misrata. The load capacity of the machine is 200 kN. The welding samples for tensile testing is shown in Figure 4. The hardness test was conducted in the High Vocational Center of Casting at Tripoli using a BMS Bulut Makina Sanayi microhardness tester. The Vickers micro-hardness test for HAZ for a sample is shown in Figure 5. The indenter used is a diamond cone with a load of 1 kg of pressure force. The indenter used is a diamond cone with a 120-degree angle. The hardness of the welding area, or FZ, was measured to demonstrate the change in the welding parameters on them. The Vickers micro-hardness value is an average of three runs taken for each sample. Table 5 shows the orthogonal array for welding parameters with their corresponding tensile strength and Vickers micro-hardness for FZ and HAZ. The microstructure was examined after transverse cross-sectioning welding samples using the Buelher® sectioning machine and then hot mounting using red phenolic resin. The grinding of samples is done with sandpaper from 80 grit to 1200 grit and then polished on a polishing mat with alumina powder as polishing liquid (0.05 µm grain size). The samples were then suspended in Nital etchant for a few seconds, and the microstructure was inspected by a Zeiss AxioCam ICC-5 optical microscope.

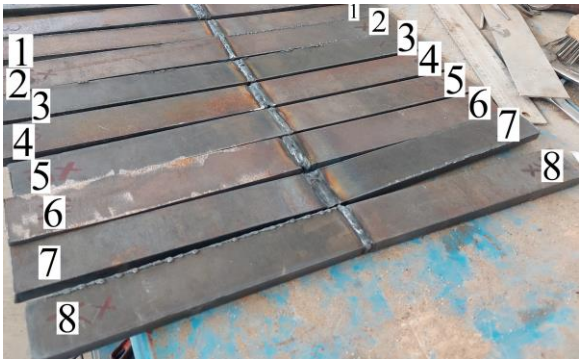

Figure 4 Tensile strength samples before testing

Figure 5 Vickers micro-hardness test for HAZ for a welding sample

3.0 RESULTS AND DISCUSSION

The observations from Table 5 indicate that the tensile strength increased with the increased Vickers micro-hardness for FZ and HAZ. For example, sample 1 obtained 305 MPa tensile strength and 2170 FZ hardness and 2311 HAZ hardness, while sample 8 showed a tensile strength of 164 MPa and 2151 VHN and 2245 VHN for FZ and HAZ, respectively. The hardness values for HAZ were higher than those for FZ as illustrated in Figure 6. However, the increased FZ hardness means harder HAZ, as reported in a previous study [29]. The tensile strength decreased with the increased heat input from 2970 J/mm to 960 J/mm, while the heat input increased with the increased welding voltage as seen in Table 5.

Table 5 Welding parameters and their corresponding tensile strength and Vickers micro-hardness

No	Voltage (volts)	WFS (m/min)	Groove shape	Tensile strength (N/mm²)	Heat input (J/mm)	Vickers micro-hardness number (VHN)		(N/mm²) / VHN (FZ)	(N/mm²) / VHN (HAZ)	EL (%)
						FZ	HAZ			
1	20	5.9	V	305	960	2170	2311	0.14	0.13	7
2	20	5.9	Double V	263	960	2158	2195	0.12	0.12	6
3	20	10.6	V	238	960	2162	2277	0.11	0.10	7
4	20	10.6	Double V	253	960	2170	2283	0.12	0.10	6
5	27.5	5.9	V	233	2970	2155	2259	0.11	0.10	6
6	27.5	5.9	Double V	190	2970	2143	2263	0.09	0.08	6
7	27.5	10.6	V	192	2970	2157	2290	0.09	0.08	7
8	27.5	10.6	Double V	164	2970	2151	2245	0.08	0.07	4

It is also noticed from Table 5 that tensile strength decreased in samples with double V-shaped welding compared to V-shaped welding samples at the same voltage and WFS except for samples 3 and 4. For example, Sample 1 had V-shaped welding that obtained 305 MPa, while Sample 2 had double V-

shaped welding that obtained 263 MPa. Both samples were welded at 20 volts and 5.9 m/min for WFS. Similar to sample 5 compared to sample 6 at 27.5 V and 5.9 m/min, and 7 compared to 8. The tensile strength to hardness ratio in Table 5 was lower for FZ and HAZ with the increased heat input and WFS.

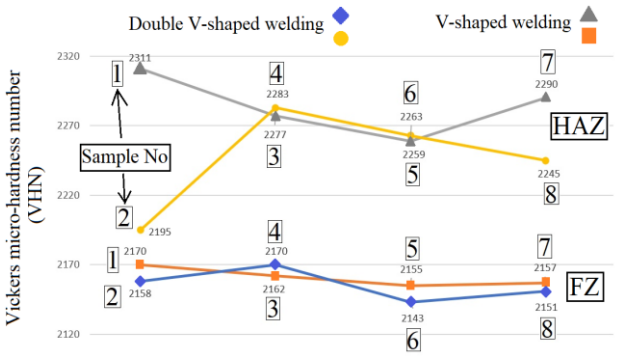

Figure 6 Graph showing Vickers micro-hardness for FZ and HAZ for V-shaped and double V-shaped welding samples

The shape of the fracture that results from the tensile test can indicate important aspects of the welding tensile properties and their relationship to the welding hardness. The samples after the tensile test have shown fractures at FZ and HAZ, as shown in Figure 7. The fracture at FZ occurred mostly in V-shaped welding samples, while most double V-shaped welding samples have experienced fracture at HAZ. This concludes that the double V-shaped welding has weaker attachment to the groove ends. It is suggested that it is related to the double V-shaped base metal groove, which is considered intrinsic. Another explanation related to the increased hardness in relation to the obtained tensile strength is shown in the decreased tensile strength to hardness ratio at double-V welding, especially at HAZ, as shown in Table 5. For example, the tensile strength value represents 12 % and 10% of the hardness value for both FZ and HAZ, respectively, in sample 4, which corresponds to double-V welding. This is compared to 11 % and 10 % for FZ and HAZ, respectively, for Sample 3, which correspond to V-shaped welding. Also comparing sample 6 with sample 5, and so on. Where the decreased tensile strength is related to the proportional increase in hardness, which incentivizes separation at the HAZ due to the difference in hardness between the HAZ and the base metal.

In Table 5 the increased heat input is associated with decreased tensile strength and hardness. A study by Lahtinen *et al*. (2019) on high strength steel agree that higher heat input promotes earlier localization of the strain and therefore lower maximum strength [30]. It also shown in Figure 6 that hardness curve for FZ and HAZ moving down slope for samples 5 to 8, although some samples has shown increased hardness. The heat input of welding was reported to affects its mechanical properties [29]. The increased heat input leads to longer cooling rates [31], which, therefore, causes increased internal stresses and residual strains in the welding [31, 32, 33]. The internal stresses have been reported to cause decreased hardness [34]. The decreased hardness was reported to result in lower transverse tensile strength [19, 20, 21]. This because the decreased hardness promotes ductility and thus decreased welding tensile strength.

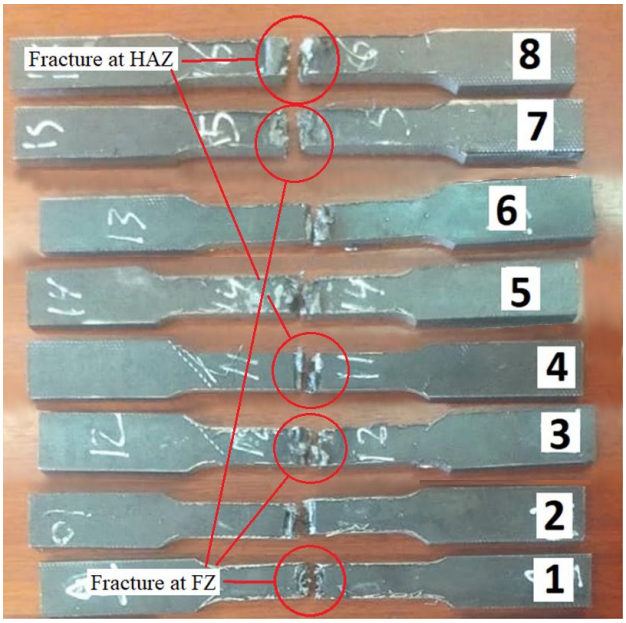

Figure 7 Tensile strength samples showing fracture at the FZ and HAZ

In Table 5, it is noticed that the Vickers micro-hardness values were close. In other words, the deviation of hardness results was smaller: 9.16 as the standard deviation for FZ hardness and 34.94 for HAZ hardness. While the tensile strength values have a standard deviation of 45.85. It indicates that the change in hardness, especially at HAZ, results in a larger impact on the welding transverse tensile strength.

The increase hardness at V-shaped welding can also relate to the interpass heat input. Since the V-shaped welding get exposed to more welding passes as shown in Figure 3. The increased welding passes was reported to increase the interpass heat input [31]. It is suggested to cause localized heat treatment around the passes boudaries since the excessive heat causes release in the internal stresses and therefore reduced hardness [35].

Figure 8 shows the microstructure of base metal magnified 20 times. The figure shows light-contrasted grains representing the conventional a-ferrite (a), and dark grains of carbide (i.e., iron carbide) colonies blended with smaller areas of perlite (P). Due to the material used having 0.17 % carbon, the carbide and perlite grains appeared less numerous

than the a-ferrite grain. Similar microstructure was obtained by Hao *et al*. (2021) in a study on A-R steel that has a close composition of 0.18 % C and 1.24 % Mn [36]. A study by Mathevon (2021) showed areas of pearlitic-rich bands called banding on steel grade 0.17 % C and 1.7 % Mn [37].

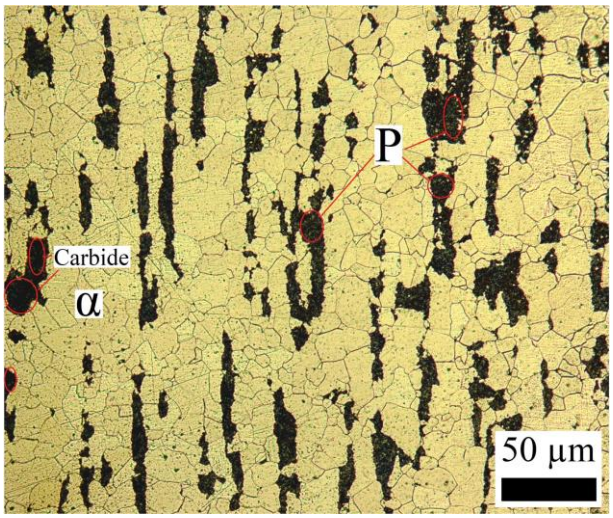

Figure 8 Base metal microstructure magnified 20 times

Figure 9 shows the microstructure of the FZ and HAZ microstructures taken in the middle of each zone magnified 20 times for V-shaped welding. The figure shows the FZ and HAZ microstructures for sample 3, Figures 9 (a) and 9 (c), respectively. Figures 9 (b) and 9 (d) show the microstructure of FZ and HAZ for sample 7, respectively. Figure 10 illustrates the microstructure for double V-shaped welding for FZ and HAZ in sample 6, as shown in Figures 10 (a) and 10 (c), respectively, while Figures 10 (b) and 10 (d) show the microstructure of FZ and HAZ in sample 8. Sample 3 and sample 7 represent welding made with a V-shaped base metal groove fabricated at 20 volts and 27.5 volts, respectively, while the WFS was fixed at 10.6 m/min. However, in samples 6 and 8, they both represent welding made in a double-V base metal groove. Both samples were exposed to a similar voltage of 27.5 volts, while the WFS changed from 5.9 m/min to 10.6 m/min. The sample numbers follow the numbering as listed in Table 5. The difference in parameter change may demonstrate the effect of the change of those parameters on the microstructure of welding and thus on its mechanical properties.

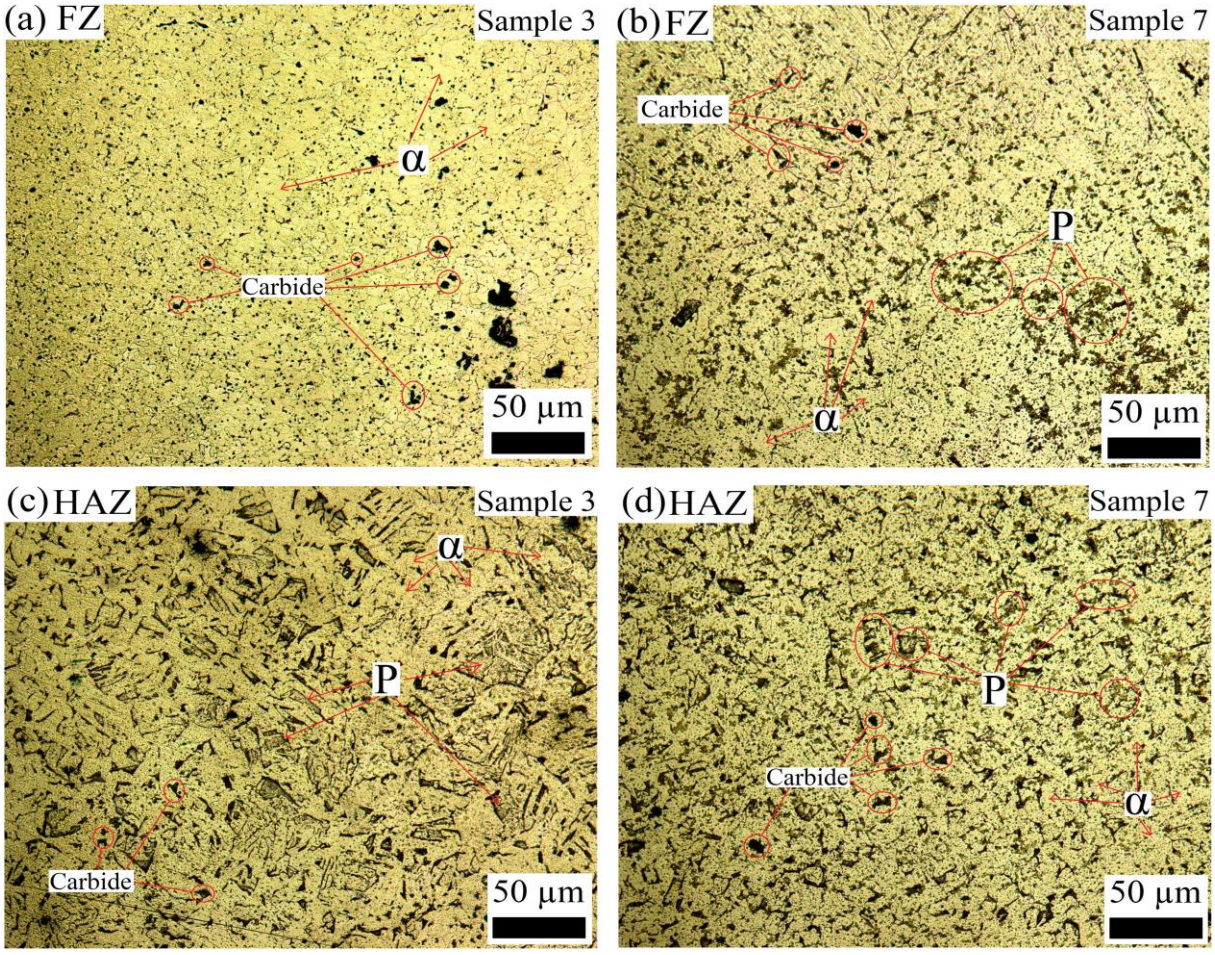

Figure 9 Microstructure of V-shaped welding magnified 20 times; (a) FZ and (c) HAZ for samples 3 at 20 volts, (b) FZ and (d) HAZ for samples 7 at 27.5 volts

The microstructure of the FZ at sample 3 (Figure 9(a)) shows carbide (i.e., iron carbide) grains spread in a matrix of fine a-ferrite, while the HAZ has shown the presence of perlite columnar dendrite grains along with coarse a-ferrite and carbide grains. The raised welding voltage of 27.5 volts at V-shaped welding resulted in a change in the FZ and HAZ microstructure, as seen in Figure 9 (b) to (d). It has shown higher precipitation of equiaxed perlite grains along with coarser a-ferrite and carbide grains at FZ (Figure 9(b)). However, the perlite columnar dendrites became less dense with increased equiaxed perlite precipitation, while a-ferrite grains became finer. A study by Mortazavian *et al*. (2020) on the C-Mn (880-grade) rail substrate has shown similar results, where an increased precipitation of perlite occurred at the HAZ [38].The microstructure of welding made with double V-shaped welding, as seen in Figure 10, showed the presence of acicular ferrite along the columnar perlite grain boundary that is called Widmanstätten ferrite along with polygonal ferrite in between in the FZ (Figure 10(a)) and HAZ (Figure 10(c)), except at HAZ the Widmanstätten ferrite was denser. Also, the HAZ showed the presence of lower bainite. These structures were presented at FZ (Figure 10(a)) and HAZ (Figure 10(c)) in sample 6. However, at an increased WFS of 10.6 m/min, the microstructure at FZ showed coarser Widmanstätten ferrite along with coarser equiaxed perlitic grains blended with carbide and a-ferrite, as shown in Figure 10(b). While at HAZ, Widmanstätten ferrite disappeared, and only equiaxed perlite blended with carbide bands separated the coarse and fine a-ferrite.

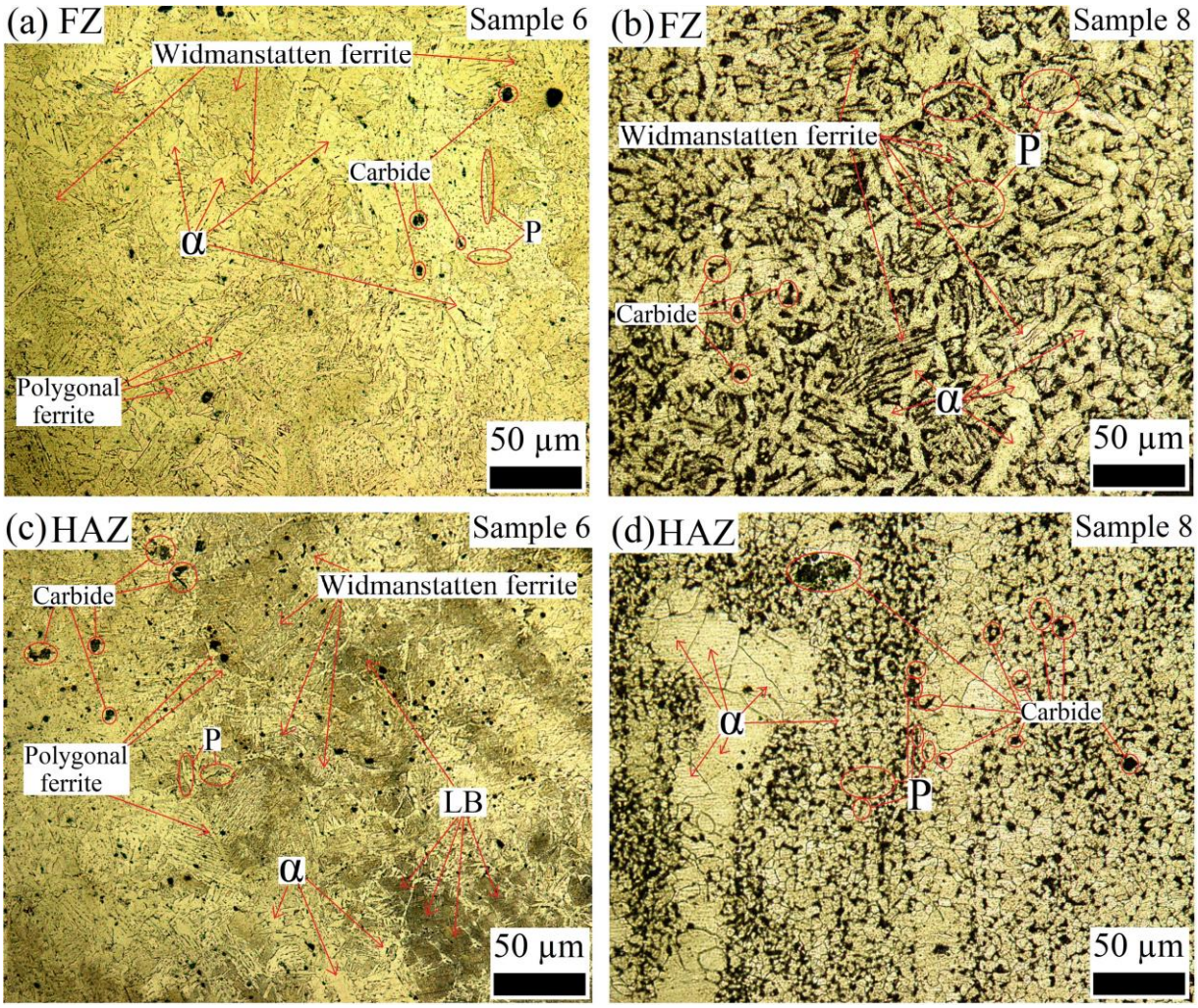

Figure 10 Microstructure of double V-shaped welding magnified 20 times; (a) FZ and (c) HAZ for samples 6 at 5.9 m/min WFS, (b) FZ and (d) HAZ for samples 8 at 10.6 m/min WFS

The increased welding voltage caused increased heat input, as shown in Table 5. The WFS was also reported to affect welding by changing the heat input and cooling rate [39]. The WFS has been shown to affect the hardness of welding (i.e., FZ and HAZ) by increasing and decreasing when comparing the samples at fixed voltage and groove shape (e.g., samples 1 showed 2170 VHN in FZ and 2311 VHN in

HAZ, while sample 3 showed 2162 VHN and 2277 VHN for FZ and HAZ, respectively) as seen in Table 5. The increased WFS has been shown to cause a decreased tensile strength to hardness ratio, which consequently affects the transverse tensile strength of welding (Table 5).

The increased welding voltage resulted in welding microstructure development, as seen in Figures 9 (b) and 9 (d). It showed an increased perlitic precipitation at FZ (Figure 9 (b)) and higher perlitic diffusion at FZ (Figure 9 (b)) and HAZ (Figure 9 (d)). The coarser a-ferrite at FZ (Figure 9(b)) is a result of higher heat input caused by increased voltage. However, the increased heat input has caused the a-ferrite to become finer at HAZ (Figure 9(b)) due to the excessive heat and longer cooling time, which have caused the a-ferrite to developed more from its original structure of base metal as shown in Figure 8 to become finer. A study by Mehta *et al*. (2021) showed similar microstructure of HAZ for AISI 1010 and showed that it appeared at temperatures around 730 °C [40] above temperature Ae1 [41]. In comparison with the microstructure of double V-shaped welding, Mehta *et al*. (2021) stated that Widmanstätten ferrite started appearing at 670 °C and below [40]. It is suggested to be due to the increased interpass heat input because of the increased welding passes that result in excessive heat at FZ, as discussed earlier. It has caused developed microstructure [42] at FZ and HAZ at V-shaped welding (Figure 9). That also explains the presence of Widmanstätten ferrite and lower bainite as seen in Figures 10 (a), 10 (b), and 10 (c). The latter was reported to form at 370 °C due to the displacive mechanism that traps most of the carbon that is caused by a strong driving force [40]. It is suggested that since each V opening of the double V-shaped groove has experienced one welding pass (Figure 3), it has been exposed to lower heat input (Table 5) than V-shaped welding and therefore has a less developed microstructure. In general, the increased WFS has resulted in higher equiaxed perlite and carbide precipitation along with coarser a-ferrite (Figure 10 (b)), while HAZ has witnessed the development of finer a-ferrite (Figure 10 (d)).

Table 5 shows higher transverse tensile strength at sample 3 when compared with sample 7. Since both the samples have V-shaped welding and experience fracture at FZ, it is suggested that this is related to the fact that sample 3 showed finer a-ferrite and lower carbide precipitation at FZ (Figure 9(a)). It is also suggested to be related that sample 3 showed higher FZ hardness (2162 VHN) compared to 2147 VHN for sample 7. Also, since the FZ showed lower hardness than in HAZ (2277 VHN for sample 3 and 2290 VHN for sample 7), it could be due to the fracture occurring in a lower hardness area (i.e., the FZ). It was reported that the increased interpass heat input that the sample 7 were exposed to reduced the welding transverse tensile strength [42]. Xue *et al*. (2021) stated that higher heat input leads to wider HAZ and reduced mechanical properties of joints [43]. The welding made a double V-shaped groove; samples 6 and 8 also have higher HAZ hardness (2263 VHN for sample 6 and 2245 for sample 8) than FZ (2143 for sample 6 and 2151 for sample 8). However, they have shown fractures at HAZ (Figure 7). It is suggested that due to the presence of Widmanstätten ferrite and lower bainite in HAZ in sample 6 (Figure 10(c)), which resulted from a lower heat input and faster cooling rate as discussed earlier, there were also increased carbide and perlite bands in the non-homogeneous microstructure as seen in Figure 10(d). It could also be due to the intrinsic shape of the double V-shaped groove in sample 8, as discussed earlier. The tensile hardness ratio to hardness was lower in samples 6 and 8 (i.e., the tensile strength value represented only 8 % of the hardness value of HAZ for samples 6 and 7 percent for sample 8), which indicates that the increased proportional hardness along with the aforementioned suggestions caused a lower transverse tensile strength.

Figures 11 and 12 present the plots for S/N ratios and mean values for the welding parameters effect on tensile strength. The S/N ratio measurement taken for "Larger is better", demonstrates the effect of welding parameters on the higher tensile and hardness values. This is because one objective of this study is to distinguish which welding parameters or parameters demonstrate an effect on higher tensile strength and hardness, thus, higher mechanical properties and better welding. The S/N for each level at each parameter is shown in Figure 11 and listed in Table 6. The welding voltage at 20 volts showed the highest S/N ratio of 48.42, followed by WFS at 5.9 m/min (47.75), while the V-shaped welding obtained a lower S/N ratio of 47.56. The welding voltage of 27.5 volts has the lowest noise ratio. The delta values in Table 6 are a result of the S/N ratio of level 1 minus the noise ratio for level 2 for each parameter. Based on delta, the voltage ranked first as the most important parameter to influence higher tensile strength, while the groove shape parameter had the lowest effect on tensile strength. Figure 12 and Table 7 also showed that 20 volts had the highest tensile strength mean of 264.8, while 27.5 volts had the lowest tensile strength mean of 194.8. The ranking, similar to the effective measurement, shows that voltage showed higher tensile strength values, while the groove shape showed the lowest. Table 8 and Table 9 show the coefficients for the S/N ratio and means, respectively. The constant value is the mean of S/N ratios, as shown in Figure 11, while each value that corresponds to each parameter level shows the accumulated S/N ratio with respect to the S/N mean value. Table 8 and Table 9 show the P-value (population value) for each level 1, which interprets the significant value for each parameter's level for the S/N ratio and means. The 20-volt level is 0.004, which means the occurrence, or chance, of tensile strength results repeating themselves is 99.6%. Which is considered significant since the significant level is 0.05 (95%). The WFS at 5.9 m/min also shows a

significant value (P-value) of 0.038, which corresponds to 96.2 % of occurrence. While the V-shaped welding level showed a non-significant value of 0.095 (90.5%). The means in Figure 12 also show the voltage at 20 and the WFS at 5.9 m/min have significant tensile strength means, while the V-shaped welding does not.

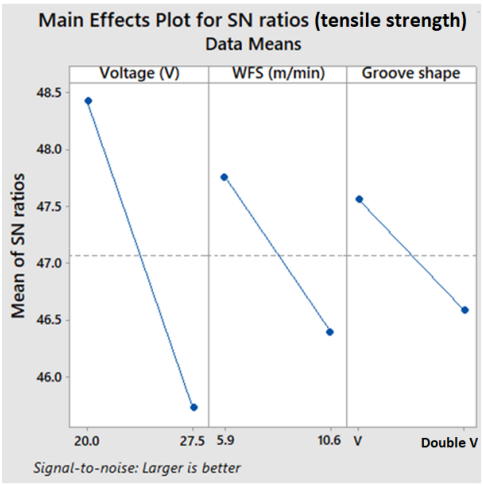

Figure 11 Plot for S/N ratio for the welding parameters for tensile strength

Table 6 S/N Ratio values for tensile strength (Larger is better)

Level	Welding voltage (volts)	WFS (m/min)	Groove shape
1	48.42	46.39	47.56
2	45.72	47.75	46.58
Delta	2.70	1.36	0.97
Rank	1	2	3

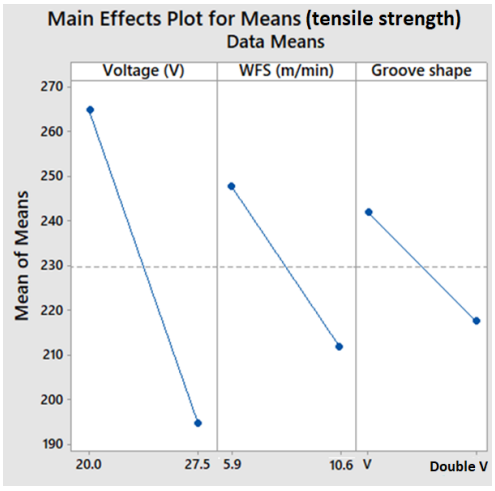

Figure 12 Plot for means for the welding parameters for tensile strength

Table 7 Mean values for tensile strength

Level	Welding voltage (volts)	WFS (m/min)	Groove shape
1	264.8	211.8	242.0
2	194.8	247.8	217.5
Delta	70.0	36.0	24.5
Rank	1	2	3

Table 8 Coefficient for S/N Ratios for tensile strength

Term	Coefficient	P
Constant	47.0705	0.000
Welding voltage (20 volts)	1.3492	0.004
WFS (5.9 m/min)	-0.6813	0.038
V-shaped base metal groove	0.4872	0.095

Table 9 Coefficient for means for tensile strength

Term	Coefficient	P
Constant	229.75	0.000
Welding voltage (20 volts)	35.00	0.004
WFS (5.9 m/min)	-18.00	0.038
V-shaped base metal groove	12.25	0.107

The WFS at 5.9 m/min showed the highest effect on hardness by showing the highest S/N ratio (66.93), as shown in Figure 13 and Table 10. It is closely followed by double V-shaped welding (66.92), while the voltage had the least effect on the hardness. The means showed similar patterns of results as shown in Figure 14 and Table 11. The WFS at 5.9 m/min has the highest mean of 2223, while the double V-shaped welding has 2221, which is considered to show a very close hardness mean. While the voltage at 27.5 showed a lower hardness mean of 2214. However, the groove shape, as ranked first in Table 10, is the most influential parameter on the hardness mean. All the parameters showed non-significance for hardness, where the P-value for 20 volts was 0.824, 0.430 for WFS at 5.9 m/min, and 0.349 for a V-shaped base metal groove.

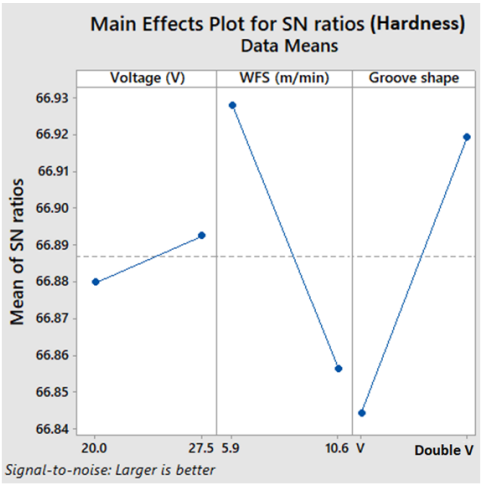

Figure 13 Plot for S/N ratio for the welding parameters for hardness

Table 10 S/N Ratio values for hardness (Larger is better)

Level	Welding voltage (volts)	WFS (m/min)	Groove shape
1	66.88	66.93	66.84
2	66.89	66.86	66.92
Delta	0.01	0.07	0.08
Rank	3	2	1

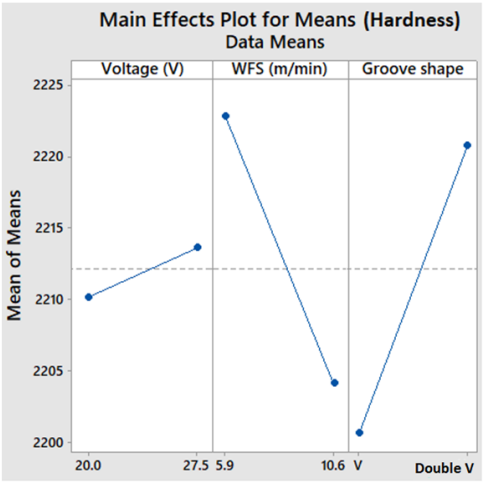

Figure 14 Plot for S/N ratio for the welding parameters for hardness

Table 11 Mean values for hardness

Level	Welding voltage (Volts)	WFS (m/min)	Groove shape
1	2210	2223	2201
2	2214	2204	2221
Delta	3	19	20
Rank	3	2	1

These results find that a welding voltage of 20 volts has the highest effect on the transverse tensile strength, followed by WFS at 5.9 m/min and a V-shaped base metal groove. Previous study on showed similar influence of voltage on the tensile strength of mild steel welding [20]. Another study by Prajapati *et al*. (2020) on the optimization of A387 alloys steel found that voltage had higher effect on welding performance characteristics [44]. The hardness is affected the most by the WFS at 5.9 m/min, followed by the double V-shaped parameter, while the voltage has the least effect on the hardness of welding (i.e., the FZ and HAZ). However, the effect of WFS on hardness was not significant. The optimum welding parameters that have obtained higher transverse tensile strength are 20 volts, 5.9 m/min, and V-shaped base metal welding. The analysis of Taguchi's design is made with the help of Minitab 18®.

4.0 CONCLUSION

In this study, mild steel was welded using GMAW under predetermined welding conditions. The weld was fabricated at a variation of voltage, WFS, and groove shape and tested for transverse tensile strength and micro-hardness along with microstructure examination. The results concluded that the tensile strength decreases with the decreased hardness and vice versa. In addition, the tensile strength and hardness were higher at welding done at a lower welding voltage (20 volts), a lower WFS (5.9 m/min), and a V-shaped base metal groove (i.e., sample 1 showed 305 MPa in welding transverse tensile strength and 2170 VHN and 2311 VHN for FZ and HAZ, respectively). The HAZ has a higher hardness than the FZ. V-shaped welding samples have experienced fracture at FZ, while double V-shaped welding showed failure at HAZ. Higher voltage (27.5 volts) and WFS (10.6 m/min) caused an increased heat input that resulted in higher internal stresses, which resulted in lower transverse tensile strength and hardness. The increased interpass heat input is due to increased welding passes for V-shaped welding. FZ has finer ferritic and perlite grains than HAZ. The HAZ has obtained Widmanstätten ferrite and lower bainite. In addition, the increased precipitation of perlite structure was present during welding, which caused lower tensile strength and hardness (i.e., sample 7 showed welding tensile strength of 192 MPa, FZ hardness of 2157 VHN, and 2290 VHN for HAZ in comparison to sample 1). Also, Widmanstatten ferrite and coarser a-ferrite were presented at welding that have a faster cooling time. Taguchi's design showed that the voltage has a higher, more significant effect on the transverse tensile strength of welding, while the WFS has shown a higher effect on welding hardness. The optimum welding parameters that have obtained higher transverse tensile strength are 20 volts, 5.9 m/min, and V-shaped base metal welding.

Conflicts of Interest

The author declares that there is no conflict of interest regarding the publication of this paper.

Acknowledgement

This work is classified under no grant scheme or scholarship. The author has provided the materials for the experimentation. The author would like to thank their families for their encouragement throughout the study. A sincere thank you goes to the Libyan Iron and Steel Company for their help. An appreciation goes to Libyan International Medical University.

References

[1] Garcia, L. M., Noronha, V.T., and Ribeiro, J. 2021. Effect of Welding Orientation in Angular Distortion in Multipass GMAW. *Journal of Manufacturing and Materials Processing*. 5(2): 63. Doi: https://doi.org/10.3390/jmmp5020063.

[2] Singh, V., Chandrasekaran, M., Samanta, S., and Thirugnanasambandam, M. 2019. Artificial Neural Network Modelling of Weld Bead Characteristics during GMAW of Nitrogen Strengthened Austenitic Stainless Steel. *AIP Conference Proceedings*. 218(1): 020024. Doi: https://doi.org/10.1063/1.5117936.

[3] Ghazvinloo, H. R., and Honarbakhsh-Raouf, A. 2021. Numerical Modeling of Heat-affected Zone in the GMAW Process. *Material Science*. 56: 807-813. Doi: https://doi.org/10.1007/s11003-021-00498-2.

[4] Jiang, Y., and Lin, P. 2019. Improvement of Numerical Simulation for GMAW based on a New Model with Thermocapillary Effect. *Journal of Computational and Applied Mathematics*. 356: 37-45. Doi: https://doi.org/10.1016/j.cam.2019.01.039.

[5] Ghazvinloo, H. R., Honarbakhsh-Raouf, A., and Shadfar, N. 2021. A Comprehensive Study on the Welded Joints Appearance in GMAW. *Journal of Materials and Environmental Science*. 12(12): 1320-1331. http://www.jmaterenvironsci.com/Journal/vol12-10.html.

[6] Prakash, S. O., Karuppusway, P., and Gandhi, B. S. 2021. Enhancing the Notch Tensile Strength of GMAW Welded AISI 1013 Low Carbon Steel with Taguchi Optimization. *A Journal of Physical Sciences, Engineering and Technology*. 13(01): 20-25. Doi: https://doi.org/10.18090/samriddhi.v13i01.5.

[7] Soltani, S., Eghtesad, M., and Bazargan-Lari, Y. 2020. Mass and Heat Transfer Control in the GMAW Process Utilizing Feedback Linearization and Sliding Mode Observer. *International Communications in Heat and Mass Transfer*. 111: 104410. Doi: https://doi.org/10.1016/j.icheatmasstransfer.2019.104410.

[8] Kumar, A. S. V., and Gandhinathan, R. 2020. Process Parameters for Metal Inert Gas Welding of Mild Steel by using Taguchi Technique–A Review. *International Journal of Material Sciences and Technology*. 10(1): 1-14. http://www.ripublication.com/ijmst20/ijmstv10n1_01.pdf.

[9] Casarini, A., Coelho, J. P., Olívio, E., Braz-César, M. T., and Ribeiro, J. E. 2020. Optimization and Influence of GMAW Parameters for Weld Geometrical and Mechanical Properties using the Taguchi Method and Variance Analysis. *ICEUBI2019 International Congress on Engineering-Engineering for Evolution*. 781-794.

[10] Ramarao, M., King, M. F. L., Sivakumar, A., Manikandan, V., Vijayakumar, M., and Subbiah, R. 2022. Optimizing GMAW Parameters to Achieve High Impact Strength of the Dissimilar Weld Joints using Taguchi Approach. *Materials Today: Proceedings*. 50: 861-866. Doi: https://doi.org/10.1016/j.matpr.2021.06.137.

[11] Casarini, A., Coelho, J. P., Olívio, E., Braz-César, M. T., and Ribeiro, J. E. 2020. Optimization and Influence of GMAW Parameters for Weld Geometrical and Mechanical Properties using the Taguchi Method and Variance Analysis. *ICEUBI2019 International Congress on Engineering-Engineering for Evolution*. 781-794. Doi: https://doi.org/10.18502/keg.v5i6.7097.

[12] Assefa, A. T., Ahmed, G. M. S., Alamri, S., Edacherian, A., Jiru, M. G., Pandey, V., and Hossain, N. 2022. Experimental Investigation and Parametric Optimization of the Tungsten Inert Gas Welding Process Parameters of Dissimilar Metals. *Materials*. 15(13): 4426. Doi: https://doi.org/10.3390/ma15134426

[13] Kalita, K., Burande, D., Ghadai, R. K., and Chakraborty, S. 2023. Finite Element Modelling, Predictive Modelling and Optimization of Metal Inert Gas, Tungsten Inert Gas and Friction Stir Welding Processes: A Comprehensive Review. *Archives of Computational Methods in Engineering*. 30(1): 271-299. Doi: https://doi.org/10.1007/s11831-022-09797-6.

[14] Ogbonna, O. S., Akinlabi, S. A., Madushele, N., Fatoba, O. S., and Akinlabi, E. T. 2023. Grey-based Taguchi Method for Multi-weld Quality Optimization of Gas Metal Arc Dissimilar Joining of Mild Steel and 316 Stainless Steel. *Results in Engineering*. 17: 100963. Doi: https://doi.org/10.1016/j.rineng.2023.100963.

[15] Om Prakash, S., Pathmasharma, S., Bharath, V., and Deivasikamani, D. M. 2019. Parameters Optimization of Gas Metal Arc Welding Process (GMAW) by using Design of Experiments. *International Journal of Technical Innovation in Modern Engineering and Science*. 5: 1-12. https://ijtimes.com/IJTIMES/index.php/ijtimes/article/view/3260.

[16] Assefa, A. T., Ahmed, G. M. S., Alamri, S., Edacherian, A., Jiru, M. G., Pandey, V., and Hossain, N. 2022. Experimental Investigation and Parametric Optimization of the Tungsten Inert Gas Welding Process Parameters of Dissimilar Metals. *Materials*. 15(13): 4426. Doi: https://doi.org/10.3390/ma15134426.

[17] Khan, M. A., and Agrawal, Y. 2022. GMAW Process Parameter Utilisation Analysis using ANOVA and Taguchi Relations. *International Journal of Engineering Research in Current Trends*. 2(3): 69-71. https://www.ijerct.com/papers/02-03/gmaw-process-parameter-utilisation-analysis-using-anova-and-taguchi-relations.pdf.

[18] Khamari, B. K., Dash, S. S., Karak, S. K., and Biswal, B. B. 2019. Effect of Welding Parameters on Mechanical and Microstructural Properties of GMAW and SMAW Mild Steel Joints. *Ironmaking and Steelmaking*. 1-9. Doi: https://doi.org/10.1080/03019233.2019.1623592.

[19] Elfallah, S. S. S. 2022. Influence of GMAW Factors on the Tensile Strength of Commercial Steel. *International Science and Technology Journal*. 6(4): 1-16. https://www.stcrs.com.ly/istj/article-details.php?id=500.

[20] Elfallah, S. 2022. Study on the Influence of Groove shape on the Tensile Strength of Commercial Steel. *Journal of Engineering Research*. 1-15. Doi: https://doi.org/10.36909/jer.18695.

[21] Elfallah, S. S. 2022. Effect of GMAW on the Tensile Strength and Hardness of Commercial Steel. *International Journal of Computer Sciences and Engineering*. 10(9): 14-20. Doi: https://doi.org/10.26438/ijcse/v10i9.1420.

[22] Calderón, L., Bohórquez, O., Rojas, M. A., and Pertuz, A. 2021. Experimental Relationship of Tensile Strength and Hardness of Welded Structural Steel. *Journal of Physics: Conference Series*. 2046(1): 012065. Doi: https://doi.org/10.1088/1742-6596/2046/1/012065.

[23] Luo, Y., Gu, W., Peng, W., Jin, Q., Qin, Q., and Yi, C. 2020. A Study on Microstructure, Residual Stresses and Stress Corrosion Cracking of Repair Welding on 304 Stainless Steel: Part I-Effects of Heat Input. *Materials*. 13(10): 2416. Doi: https://doi.org/10.3390/ma13102416.

[24] Sabry, I. 2021. Experimental and Statistical Analysis of Possibility Sources–rotation Speed, Clamping Torque and Clamping Pith for Quality Assessment in Friction Stir Welding. *Management and Production Engineering Review*. 12(3): 84-96. Doi: https://doi.org/10.24425/mper.2021.138533.

[25] Sankar, N., Malarvizhi, S., and Balasubramanian, V. 2021. Mechanical Properties and Microstructural Characteristics of Rotating Arc-gas Metal Arc Welded Carbon Steel Joints. *Journal of the Mechanical Behavior of Materials*. 30(1): 49-58. Doi: https://doi.org/10.1515/jmbm-2021-0006.

[26] ASTM. 2022. Standard Test Methods for Tension Testing of Metallic Materials. E8/E8M-22. Doi: https://doi.org/10.1520/E0008_E0008M-22.

[27] World Material. 2023. EN 1.0038 steel S235JR Material

Equivalent, Properties, Composition. Information on https://www.theworldmaterial.com/1-0038-steel-s235jr-material/.
[28] Weld Wire. 2023. ER70S-6 welding wire data sheet. Information on https://www.weldwire.net/weld_products/ww70s-6/.
[29] Ahmed, M. M., Ataya, S., El-Sayed Seleman, M. M., Mahdy, A. M., Alsaleh, N. A., and Ahmed, E. 2020. Heat Input and Mechanical Properties Investigation of Friction Stir Welded aa5083/aa5754 and aa5083/aa7020. *Metals*. 11(1): 68. Doi: https://doi.org/10.3390/met11010068.
[30] Lahtinen, T., Vilaça, P., Peura, P., and Mehtonen, S. 2019. MAG Welding Tests of Modern High Strength Steels with Minimum Yield Strength of 700 MPa. *Applied Sciences*. 9(5): 1031. Doi: https://doi.org/10.3390/app9051031.
[31] Scharf-Wildenhain, R., Haelsig, A., Hensel, J., Wandtke, K., Schroepfer, D., Kromm, A., and Kannengiesser, T. 2022. Influence of Heat Control on Properties and Residual Stresses of Additive-Welded High-Strength Steel Components. *Metals*. 12(6): 951. Doi: https://doi.org/10.3390/met12060951.
[32] Vemanaboina, H., Sridhar Babu, B., Gundabattini, E., Ferro, P., and Kumar, K. 2021. Effect of Heat Input on Distortions and Residual Stresses Induced by Gas Tungsten Arc Welding in SS 316L to INCONEL625 Multipass Dissimilar Welded Joints. *Advances in Materials Science and Engineering*. 2021. Doi: https://doi.org/10.1155/2021/1028461.
[33] Alhafadhi, M. H., and Krallics, G. 2019. The Effect of Heat Input Parameters on Residual Stress Distribution by Numerical Simulation. *IOP Conference Series: Materials Science and Engineering*. 613(1): 012035. Doi: https://doi:10.1088/1757-899X/613/1/012035.
[34] Ji, H., Gupta, M. K., Song, Q., Cai, W., Zheng, T., Zhao, Y., and Pimenov, D. Y. 2021. Microstructure and Machinability Evaluation in Micro Milling of Selective Laser Melted Inconel 718 Alloy. *Journal of Materials Research and Technology*. 14: 348-362. Doi: https://doi.org/10.1016/j.jmrt.2021.06.081.
[35] Sridharan, N., Bunn, J., Kottman, M., Fancher, C. M., Payzant, A., Noakes, M., and Babu, S. S. 2021. Consumable Development to Tailor Residual Stress in Parts Fabricated using Directed Energy Deposition Processes. *Additive Manufacturing*. 39: 101837. Doi: https://doi.org/10.1016/j.addma.2021.101837.
[36] Hao, X., Zhao, X., Chen, H., Huang, B., Ma, J., Wang, C., and Yang, Y. 2021. Comparative Study on Corrosion Behaviors of Ferrite-pearlite Steel with Dual-phase Steel in the Simulated Bottom Plate Environment of Cargo Oil Tanks. *Journal of Materials Research and Technology*. 12: 399-411. Doi: https://doi.org/10.1016/j.jmrt.2021.02.095.
[37] Mathevon, A. 2020. Characterization and Modelling of Microstructural Evolutions and Mechanical Properties during the Thermal Treatments of Dual-Phase Steels. Doctoral Dissertation, Université de Lyon. https://theses.hal.science/tel-03186693/.
[38] Mortazavian, E., Wang, Z., and Teng, H. 2020. Repair of Light Rail Track through Restoration of the Worn Part of the Railhead using Submerged Arc Welding Process. *The International Journal of Advanced Manufacturing Technology*. 107(7-8): 3315-3332.
[39] Doi: https://doi.org/10.1007/s00170-020-05208-x.
[40] Yin, X., He, G., Meng, W., Xu, Z., Hu, L., and Ma, Q. 2020. Comparison Study of Low-heat-input Wire Arc-fabricated Nickel-based Alloy by Cold Metal Transfer and Plasma Arc. *Journal of Materials Engineering and Performance*. 29: 4222-4232. Doi: https://doi.org/10.1007/s11665-020-04942-3.
[41] Mehta, Y., Rajput, S. K., and Kumar, S. 2021. Establish Time-temperature-transformation Diagram based on Dilatometry Results and Microstructural Evolutions in an AISI 1010 Steel. *Indian Journal of Engineering and Materials Sciences*. 28(3): 234-239. Doi: https://doi.org/10.56042/ijems.v28i3.45776.
[42] Poyraz, O., and Ögel, B. 2020. Recrystallization, Grain Growth and Austenite Formation in Cold Rolled Steels during Intercritical Annealing. *Journal of Materials Research and Technology*. 9(5): 11263-11277. Doi: https://doi.org/10.1016/j.jmrt.2020.08.015.
[43] de Oliveira Moraes, D., Júnior, P. Z., e Oliveira, V. H. P. M., de Oliveira, A. C., and da Cruz Payão Filho, J. 2022. Effect of the Girth Welding Interpass Temperature on the Toughness of the HAZ of a Ni-based Superalloy 625 Clad API 5L X65 Pipe Welded Joint. *Journal of Materials Research and Technology*. 19: 2556-2566. Doi: https://doi.org/10.1016/j.jmrt.2022.05.141.
[44] Xue, J., Peng, P., Guo, W., Xia, M., Tan, C., Wan, Z., and Li, Y. 2021. HAZ Characterization and Mechanical Properties of QP980-DP980 Laser Welded Joints. *Chinese Journal of Mechanical Engineering*. 34(1): 80. Doi: https://doi.org/10.1186/s10033-021-00596-x.
[45] Prajapati, V., Vora, J. J., Das, S., and Abhishek, K. 2020. Study of Parametric Influence and Welding Performance Optimization during Regulated Metal Deposition (RMD™) using Grey Integrated with Fuzzy Taguchi Approach. *Journal of Manufacturing Processes*. 54: 286-300. Doi: https://doi.org/10.1016/j.mtcomm.2023.105401.